Acta Scientiarum
http://periodicos.uem.br/ojs
ISSN on-line: 1807-8664
Doi: 10.4025/actascitechnol.v46i1.66600

Characterization of SnO_2-based gas sensors to analyze diesel and biodiesel blends

Leonardo Tadeu Boaes Mendonça[1,2*], Nazaré do Socorro Lemos Silva Vasconcelos[4], Marcelo Moizinho Oliveira[4], José Hilton Gomes Rangel[4] and Jomar Sales Vasconcelos[3]

[1]Programa de Pós graduação em Engenharia de Materiais, Instituto Federal do Maranhão, Av. Getúlio Vargas, 65030-005, São Luis, Maranhão, Brasil. [2]Departamento de Tecnologia Química, Universidade Federal do Maranhão, Av. dos Portugueses, Vila Bacanga,65080-805, São Luis, Maranhão, Brasil. [3]Departamento de Engenharia Elétrica, Instituto Federal do Maranhão, São Luis, Maranhão, Brasil. [4]Departamento Acadêmico de Química, Instituto Federal do Maranhão, São Luis, Maranhão, Brasil. *Author for correspondence. E-mail: leonardo.boaes@ufma.br

ABSTRACT. This study analyzed biodiesel blends using sensors constituted by SnO_2 pellets with gold interdigitated contacts deposited on the surface. Tin dioxide was synthesized by the polymeric precursor method with further calcination treatment at 500°C, conformed and sintered at three temperatures to form three different samples: 700°C (Sn1), 900°C (Sn2) and 1100°C (Sn3). The samples were analyzed by X-Ray Diffraction, FEG-SEM (Field Emission Gun - Scanning Electron Microscopy), Raman spectroscopy, and electrical measurements. Results confirmed the formation of rutile-type tetragonal cassiterite phase, with quasi-spherical particles a moderate degree of heterogeneity in particle size 30-90 nm). Raman vibrational modes and infrared spectrum also confirmed the presence of tin oxide in high purity rutile phase. Sensorial measurements showed high sensitivity, response, and recovery time in tests with biodiesel/ethanol mixtures, allowing to distinguish between blends with a wide range of composition and serving as a potential device to detect adulterated fuel.

Keywords: gas sensor; tin dioxide; blends; biodiesel; ethanol; diesel.

Received on January 09, 2023.
Accepted on January 11, 2024.

Introduction

The evergoing search for high-quality analytical devices has fueled studies on portable, fast-response, high-sensitivity materials. Gas sensors fit these requirements and are highly selective to gases and volatile compounds. These sensors interact with gases and vapors altering their intrinsic properties, such as electrical resistance, luminescence, and piezoelectricity. Gas sensors are widely used to detect toxic and flammable vapors (Park et al., 2019), pollutants (Hong et al., 2019), alcohol oxidation in beverages (Moriaux et al., 2018) and contamination of edible oils (Cai, Goo, & Park, 2021; Feng et al., 2021; Sihombing & Alfarandi Ritonga, 2021).

Metal oxides present high sensibility, stability and performance in short-time analysis. Sensor sensitivity is affected by particle size, concentration and molecular structure. Many studies have focused on improving sensor sensitivity by doping or forming composites (Bianchetti. Arrieta, & Wälson De Reca, 2015; Park et al., 2019).

Since its application in residential gas leak detectors back in the 1960s, tin oxide (SnO_2) has attracted considerable attention from the scientific community due to its unique sensing properties and has been employed across many industrial sectors. And as SnO_2 is an abundant mineral, it is also a low-cost material.

The sensing properties of tin oxide are yet to be fully understood, but some studies indicate that when tin oxide interacting with oxidizing and reducing gases or vapors, physical and chemical adsorption and desorption of these volatile compounds on sensor surface can alter their electrical resistance of such compounds (Cheng, Wang, Li, Liu, & Li, 2016).

This study used the Pechini method (Pechini, 1967) to obtain nanostructured SnO_2 pellets suitable for use as gas sensors with interdigitated gold electrodes to analyze ethanol content in biodiesel samples and biodiesel content in diesel samples.

Material and methods

Reagents

The reagents used for the synthesis were tin chloride dihydrate ($SnCl_2.2H_2O$. Vetec), citric acid monohydrate PA. ($C_6H_8O_7.H_2O$, Vetec) and ethylene glycol ($C_2H_6O_2$, Dinâmica). All regents used were analytical grade and without further purification.

Experimental Procedure

Tin chloride was completely solved in distilled water with further addition of citric acid in 3:1 molar ratio (citric acid: tin metal) under stirring. After complete solubilization of metal citrate, ethylene glycol was added in a weight ratio of 60:40 (citric acid: ethylene glycol). The mixture was heated and stirred for 5 hours until polyester formation.

The polymeric resin was thermally treated at 500°C for 3 hours and then powdered on agate mortar. The powder was pressed into 20 mm diameter pellets by uniaxial compression. Finally, the pellets were isostatically treated at 15 MPa and three different temperatures (700°C (Sn1), 900°C (Sn2), and 1100°C (Sn3)) at a rate of 10°C. min^{-1}.

The electrodes were deposited by sputtering using an aluminum coating to form an interdigitated pattern on the surface of the pellets. X-ray diffraction analysis was conducted using a RINT 2000 Rigaku diffractometer with Cu-Kα as the radiation source ($\lambda_{CuK\alpha}$ = 1.5418 Å) and 2θ scanning from 20° to 90°.

Electron microscopy was carried out using a FEG-SEM JEOL operated at 5 kV. Samples were prepared through particle deposition on carbon strip placed on aluminum stub holder and covered with a thin carbon layer. Micro-Raman (MR) spectroscopy was conducted on a Horiba Jobin-Yvon (Japan) spectrometer operating at 514.5 nm using Ar-ion laser (MellesGriot, United States) as excitation source.

The set-up gas sensor consisted of a Teflon chamber (7500 cm^3) with a sample holder placed internally as support for two electric resistances. One electrical resistance heats the sensor and the other vaporizes the analyte to be detected. For each analysis, the corresponding volumes were inserted into a beaker and heated until complete vaporization and the vapor was removed using a vacuum pump. Assays were performed by applying 9V with a common battery to the sensor and resistance was measured using a 20 TRMS Homis digital multimeter model. Sensor response was calculated by Equation 1:

$$S=R_{air}/R_{gas} \quad \text{(Eq. 1)}$$

Where: R_{air} represents the resistance value in the air at 300°C and R_{gas} the resistance value in the presence of vapor.

Sensitivity is defined by the mean maximum response of the sensors. Response time is the time required to achieve maximum response, and the concentration was calculated according to the volume added in the chamber divided by its volume (ppm).

Biodiesel samples were obtained by conventional esterification using babassu oil (*Attalea Speciosa*) as raw material. The blends composition (v/v) were as follows: Pure biodiesel, 2% ethanol/biodiesel (AB2), 5% ethanol/biodiesel (AB5) and pure ethanol. Diesel and biodiesel blends followed a similar pattern: pure diesel, 1% biodiesel/diesel (B1), 5% biodiesel/diesel (B5), 20% biodiesel/diesel (B20) and pure biodiesel.

Results and discussion

Characterization

X-ray diffraction analysis reveals predominant (110), (101), and (211) planes in all samples (Figure 1a). The narrow peaks shown in the diffractogram configure a clear evidence of the crystallinity of the samples. Furthermore, all peaks are indexed to cassiterite (JCPDS no. 77-449), confirming that our methodology effectively obtained the crystalline phase (Cheng et al., 2016; Tombak, Ocak, & Bayansal, 2019; Yang, Ren, Ma, Hao, & Ji, 2015). Raman spectra show vibrational modes attributed to rutile-type tetragonal SnO_2 at 774, 650, and 470 cm^{-1} associated to E_g, A_{1g} and B_{2g}, respectively (Desimone, Schipani, Procaccini, Mirabella, & Aldao, 2022; Maksimova et al., 2021). The vibrational mode at 578 cm^{-1} corresponds to A_s mode associated with oxygen vacancies and the number of vibrational modes decrease as the temperature increases (Wang et al., 2017).

SEM images show particles with quasi-spherical morphology and indicates that particle size increases as the temperature rises. We counted 500 particles, approximately, using Image J software, and particle diameters were estimated at 35 nm (Sn1), 70 nm (Sn2) and 95 nm (Sn3), confirming nanometer scale for all samples. Voids between particles suggest porosity even at high sintering temperatures (Figs. 1c, 1d, and 1e). The open paths associated with closed pores can favor gas permeability and reach the active sites of the sensor. Such behavior illustrates the challenge associated with compacting SnO_2-based ceramics (Lee, Sahu, Hajra, Mohanta, & Kim, 2021).

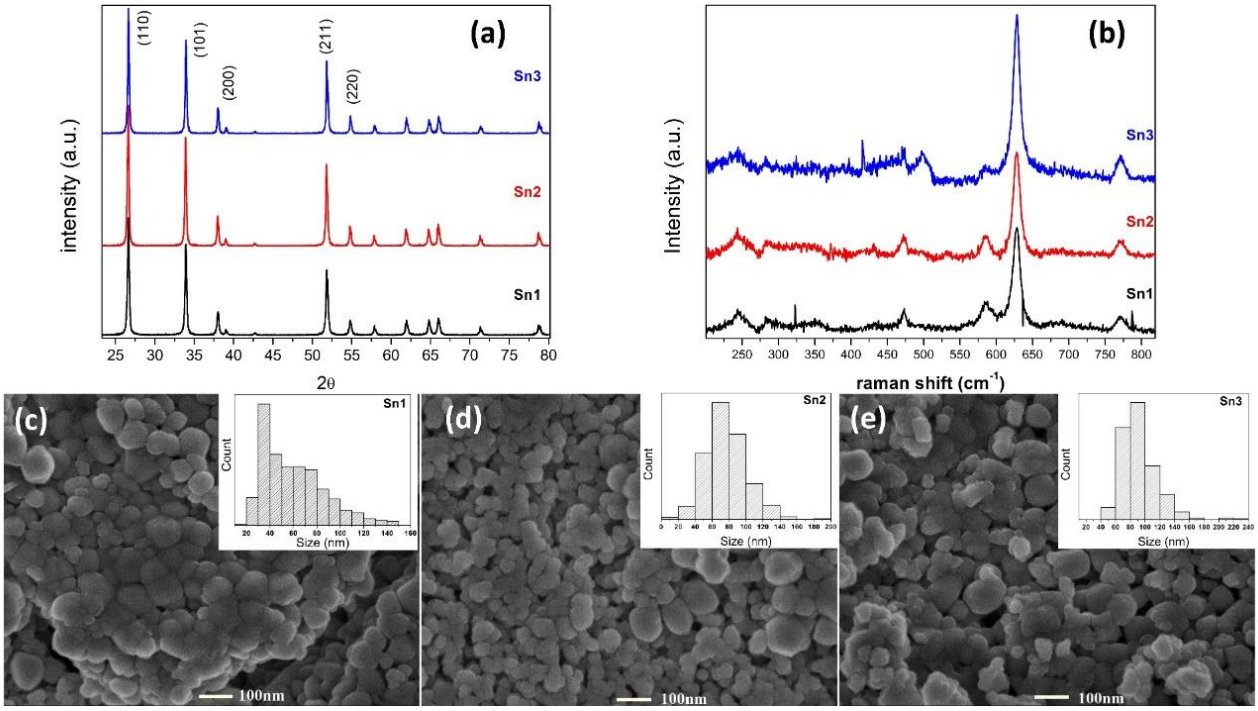

Figure 1. (a) XRD pattern of SnO_2 (b) Raman spectrum and SEM image (c) Sn1 (d) Sn2 (e) Sn3 samples (inset: histogram distribution size).

Figure 2a shows the infrared spectra for the three samples and the main vibration modes for tin oxide. The signal at 707 cm^{-1} is associated with the stretching of the Sn-O bond. Vibrations at 624 and 519 cm^{-1} correspond to O-Sn-O symmetric and antisymmetric stretching (Barakat, Shaban, & El Sayed, 2018). The presence of this mode agrees with XRD results and confirms structural order and lack of contamination, showing that the procedure applied eliminated any by-products. Crystallite size, calculated by the Scherrer equation, is plotted as a function of sintering temperature (Figure 2b). An increase in size from 30.2 to 36.1 nm was observed due to the low diffusibility of the species present in the oxide, associated with the strong Sn-O bonds.

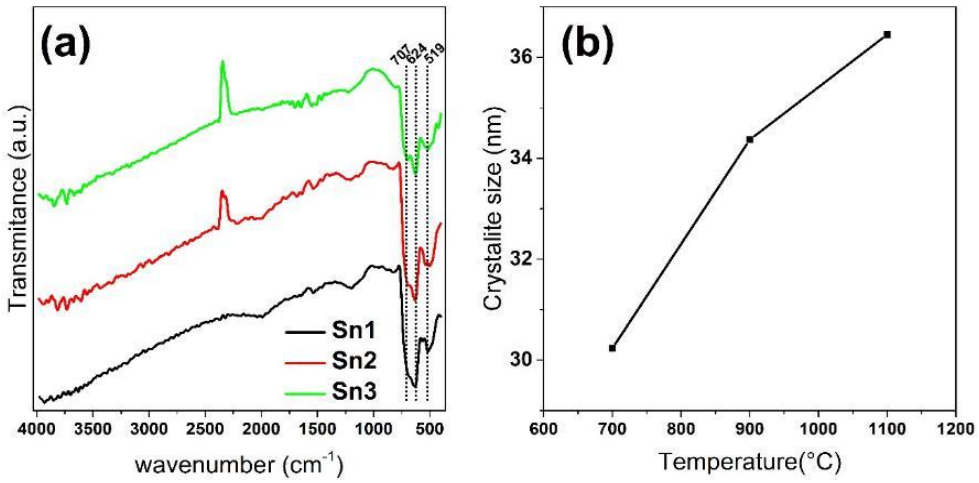

Figure 2. (a) tin oxide infrared spectrum and (b) crystallite size variation vs. sintering temperature.

Gas sensor tests

Figure 3a exhibits the relation between electrical conductivity and temperature, showing that electrical conductivity of the samples increases with the temperature up to 300°C under ambient conditions. This behavior is related to oxygen molecules adsorbed on the surface of tin oxide. Higher temperatures (100°C < T < 300°C) can generate oxygen species (O^{2-}) that increase the conductivity of metal oxides by decreasing layer depletion, thus in this range of temperature electrons are released to the conduction band (Li, Zhang, Pan, Tang, & Yu, 2022). The sintered samples exhibited great current variation, with the highest values at 300°C.

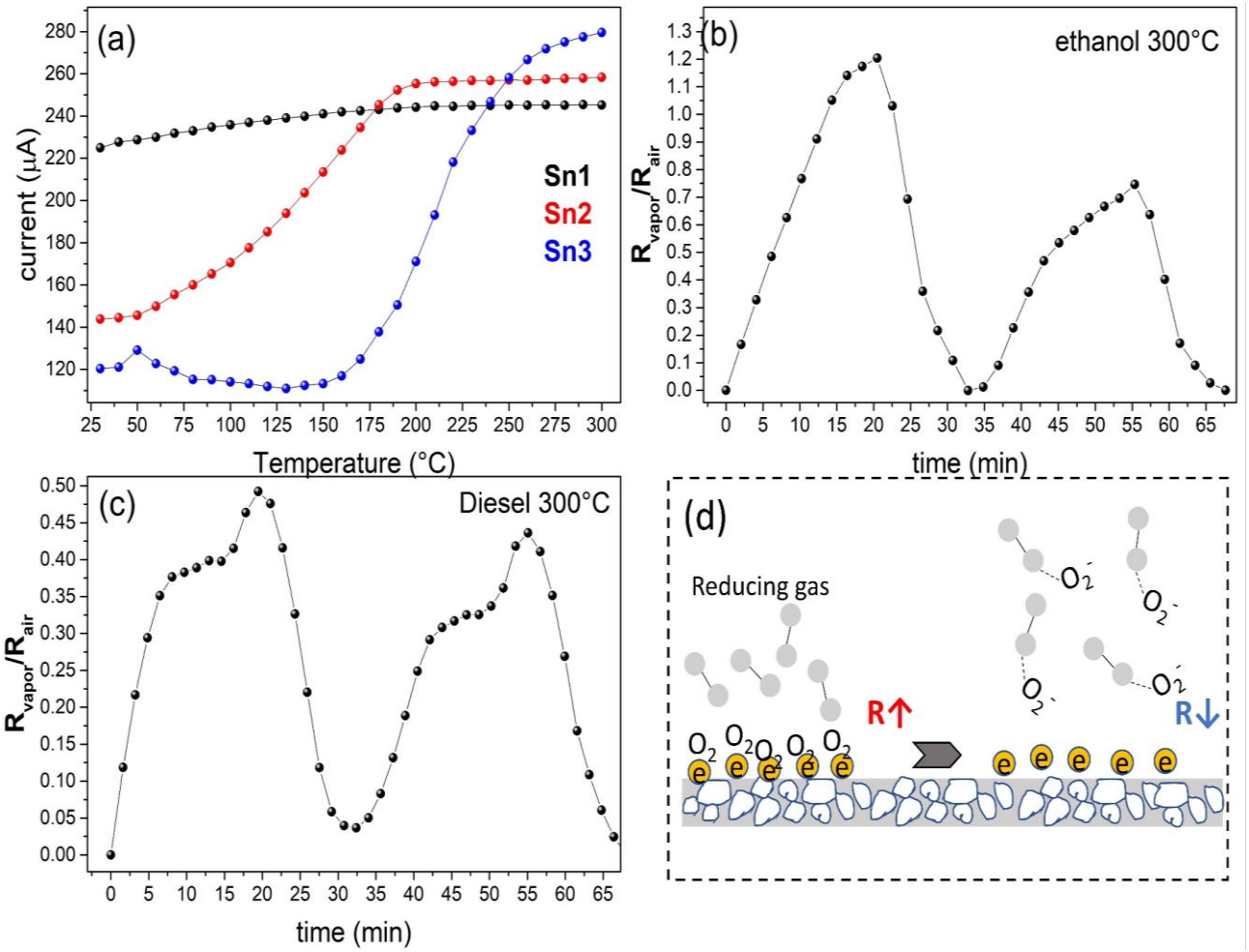

Figure 3. (a) Current x Temperature (C x I), (b) Sensitivity to ethanol (100 ppm) and (c) Diesel (10 ppm) at 300ºC (d) mechanism of action of the sensors.

The samples of tin oxide show almost same response to ethanol (Figure 3b) that could be understand by ethanol molecules adsorption on SnO_2 surface and dissociation to the hydroxyl part of the chain. At 300°C, O_2^- species is the main adsorbed on the SnO_2 surface. On one reaction route, this species reacts with hydroxyl alcohol (C_2H_5OH) removing hydrogen and releasing electrons to form acetaldehyde (CH_3CHO). On the other route ethanol is adsorbed on the surface and dissociated and then it reacts with the oxygen of oxide lattice, promoting electrons in the conduction band (Cai et al., 2021; Feng et al., 2021).

The Sn3 sample showed the most intense response to diesel, due to its more coalesced particles compared to the other samples and consequently higher mobility electrical response. These phenomena could be understood by the higher electrical mobility.

Our tests revealed that signal values increase linearly with ethanol content in biodiesel (Figure 4b and 4d). The AB5 sample presented a sensitivity increase of about 30% compared to AB2, allowing us to distinguish between the samples. This behavior is explained by the high sensibility to ethanol compared to biodiesel, which is expelled quickly and reacts with the sensors.

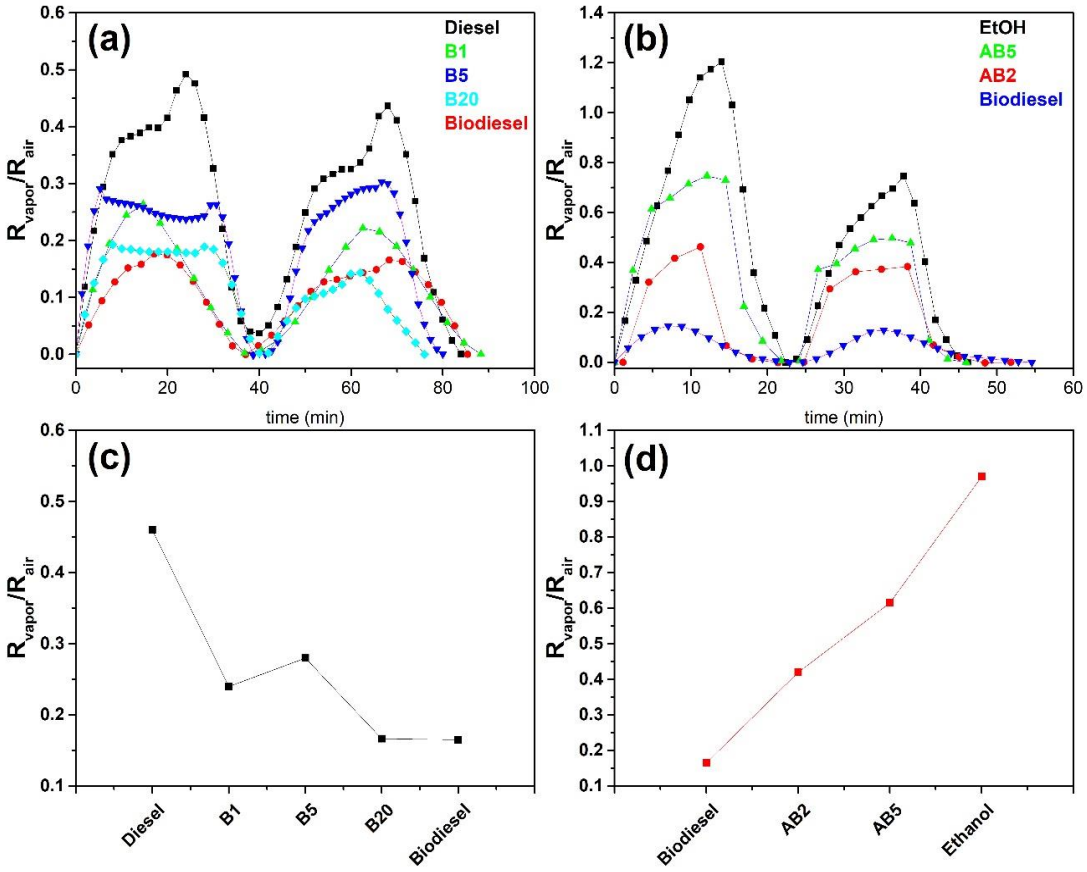

Figure 4. (a)/(c) Sensitivity to biodiesel/diesel (15 ppm) and (b)/(d) sensitivity to ethanol/biodiesel blends (2 ppm each sample).

Our findings did not show significant differences between the biodiesel/diesel blends analyzed due to their highly similar composition (Figures 4a and 4c). Adjusting the gas sensor to increase sensitivity may be able to help in this regard.

Conclusion

The methodology employed in this study successfully produced SnO_2-based gas sensors sensible to ethanol/biodiesel and biodiesel/diesel blends using nano-sized ceramic powders (< 100 nm size). Our sensors presented high sensitivity to ethanol/biodiesel blends, allowing differentiation of the samples. Sensor samples obtained at 1100°C performed better in analyses of biodiesel/ethanol blends due to their linear response variation.

Acknowledgments

The authors acknowledge the financial and technical support provided by CNPq, Capes, Fapema, IFMA, and INCTMN Liec.

References

Barakat, M. A. Y., Shaban, M., & El Sayed, A. M. (2018). Structural, ultrasonic and spectroscopic studies of tin oxide thin films; Effect of Ir and (Ni, Ir) double doping. *Materials Research Express*, *5*(6). DOI: https://doi.org/10.1088/2053-1591/aac80a

Bianchetti, M. F., Arrieta, C. L., & Walsöe De Reca, N. E. (2015). Microstructural study of nanocrystalline pure and doped tin dioxide to be used for resistive gas sensors. *Sensors and Actuators, B: Chemical*, *217*, 113–118. DOI: https://doi.org/10.1016/j.snb.2014.10.104

Cai, Z., Goo, E., & Park, S. (2021). Synthesis of tin dioxide (SnO2) hollow nanospheres and its ethanol-sensing performance augmented by gold nanoparticle decoration. *Journal of Alloys and Compounds*, *883*. DOI: https://doi.org/10.1016/j.jallcom.2021.160868

Cheng, J. P., Wang, J., Li, Q. Q., Liu, H. G., & Li, Y. (2016). A review of recent developments in tin dioxide composites for gas sensing application. *Journal of Industrial and Engineering Chemistry*, *44*, 1–22. DOI: https://doi.org/10.1016/j.jiec.2016.08.008

Desimone, P. M., Schipani, F., Procaccini, R., Mirabella, D. A., & Aldao, C. M. (2022). Evaluating the power-law response for tin dioxide nanostructured sensors in the presence of oxygen and reducing gases. *Sensors and Actuators B: Chemical*, *370*. DOI: https://doi.org/10.1016/j.snb.2022.132387

Feng, B., Feng, Y., Qin, J., Wang, Z., Zhang, Y., Du, F., ... Wei, J. (2021). Self-template synthesis of spherical mesoporous tin dioxide from tin-polyphenol-formaldehyde polymers for conductometric ethanol gas sensing. *Sensors and Actuators, B: Chemical*, *341*. DOI: https://doi.org/10.1016/j.snb.2021.129965

Hong, S., Hong, Y., Jeong, Y., Jung, G., Shin, W., Park, J., ... Lee, J. H. (2019). Improved CO gas detection of Si MOSFET gas sensor with catalytic Pt decoration and pre-bias effect. *Sensors and Actuators B: Chemical*, *300*. DOI: https://doi.org/10.1016/j.snb.2019.127040

Lee, K., Sahu, M., Hajra, S., Mohanta, K., & Kim, H. J. (2021). Effect of sintering temperature on the electrical and gas sensing properties of tin oxide powders. *Ceramics International*, *47*(16), 22794–22800. DOI: https://doi.org/10.1016/j.ceramint.2021.04.298

Li, T., Zhang, D., Pan, Q., Tang, M., & Yu, S. (2022). UV enhanced NO2 gas sensing at room temperature based on coral-like tin diselenide/MOFs-derived nanoflower-like tin dioxide heteronanostructures. *Sensors and Actuators B: Chemical*, *355*. DOI: https://doi.org/10.1016/j.snb.2021.131049

Maksimova, N. K., Sevastyanov, E. Y., Chernikov, E. V., Korusenko, P. M., Nesov, S. N., Kim, S. V., ... & Sokolov, D. V. (2021). Sensors based on tin dioxide thin films for the detection of pre-explosive hydrogen concentrations. *Sensors and Actuators, B: Chemical*, *341*. DOI: https://doi.org/10.1016/j.snb.2021.130020

Moriaux, A. L., Vallon, R., Cilindre, C., Parvitte, B., Liger-Belair, G., & Zeninari, V. (2018). Development and validation of a diode laser sensor for gas-phase CO2 monitoring above champagne and sparkling wines. *Sensors and Actuators, B: Chemical*, *257*, 745–752. DOI: https://doi.org/10.1016/j.snb.2017.10.165

Park, K. R., Cho, H. B., Lee, J., Song, Y., Kim, W. B., & Choa, Y. H. (2019). Design of highly porous SnO2-CuO nanotubes for enhancing H2S gas sensor performance. *Sensors and Actuators B: Chemical, 302*. DOI: https://doi.org/10.1016/j.snb.2019.127179

Pechini, M. P. (1967). *Method for preparing lead and alkaline earth titanates and niobates and coating method using the same to form a capacitor* (Patent 3330697).

Sihombing, Y. A., & Alfarandi Ritonga, M. (2021). Detection of the cooking oil aroma by using a gas sensor in an electronic nose system. *Journal of Physics: Conference Series*. DOI: https://doi.org/10.1088/1742-6596/1811/1/012105

Tombak, A., Ocak, Y. S., & Bayansal, F. (2019). Cu/SnO2 gas sensor fabricated by ultrasonic spray pyrolysis for effective detection of carbon monoxide. *Applied Surface Science*, *493*, 1075–1082. DOI: https://doi.org/10.1016/j.apsusc.2019.07.087

Wang, X., Wang, X., Di, Q., Zhao, H., Liang, B., & Yang, J. (2017). Mutual effects of fluorine dopant and oxygen vacancies on structural and luminescence characteristics of F doped SnO 2 nanoparticles. *Materials*, *10*(12). DOI: https://doi.org/10.3390/ma10121398

Yang, Y., Ren, S., Ma, S., Hao, C., & Ji, M. (2015). Hollow Tin Dioxide Microspheres With Multilayered Nanocrystalline Shells for Pseudocapacitor. *Electrochimica Acta*, *155*, 437–446. DOI: https://doi.org/10.1016/j.electacta.2014.12.166